Optimal Photovoltaic Energy Harvesting System at Remote Seismic Node

Dauda Duncan
Botswana International University of Science and Technology
Adamu Murtala Zungeru (zungerum@biust.ac.bw)
Botswana International University of Science and Technology
Mmoloki Mangwala
Botswana International University of Science and Technology
Bakary Diarra
University of Sciences, Techniques and Technologies of Bamako (USTTB)

Research Article

Keywords: Photovoltaic Energy Harvesting System, remote seismic node, DC-DC converter

Posted Date: July 24th, 2021

DOI: https://doi.org/10.21203/rs.3.rs-728775/v1

Optimal Photovoltaic Energy Harvesting System at Remote Seismic Node

Dauda Duncan[1], Adamu Murtala Zungeru[1], Mmoloki Mangwala[1], Bakary Diarra[2]

[1]Department of Electrical, Computer and Telecommunications Engineering, Botswana International University of Science and Technology, Private Bag 16, Palapye, Botswana

[2]Department of Electrical Engineering, Institute of Applied Sciences, University of Sciences, Techniques and Technologies of Bamako (USTTB), BP E423, Bamako, Mali.

zungerum@biust.ac.bw **(Corresponding author)**

ABSTRACT

We have developed an optimal Photovoltaic Energy Harvesting System at the remote seismic node to sustain the remote seismic node. This node is a continuous application for monitoring the geodynamics of the earth for long-term and persistent. However, due to the constraints of solar cells and low funding of seismic installations, a simple and optimal energy harvesting system is required at the remote seismic node. So, this novel design focuses on using fitting curve equations as models to extract parameters of the photovoltaic module. This is to predict instantaneous duty cycle levels across synchronous buck DC-DC converter for optimal energy conversion. The converter regulates the supercapacitor as energy storage to deliver longer runtime at the remote seismic node. The conventional techniques concentrate on improving the hardware and charging to sustain power at the remote seismic node. Yet, energy is lost by the DC-DC converter, and the lead-acid battery usually used exhibits energy leakage and a shorter lifecycle. Thus, the contribution of this work is to design a relatively less computational maximum power point tracking based on a simple curve fitting technique to sustain the lifecycle of the node. In this proposed design, selected light-dependent resistors to mimic a pyranometer and formulate equations from specific photovoltaic module characteristics are considered. This correlates the optimal duty cycle levels with the ambient irradiance and temperature variables, while validation was done with an experimental setup of Computer Controlled Photovoltaic System. The non-linear characteristics relationship between the irradiance, temperature, and voltage levels is linearized with the selected PV module parameters in curve fitting equation models. These models are implemented in C programming as an algorithm to be processed by 8-bit microcontroller and deliver duty cycle levels across pulse width modulation to drive the converter. The performance of our approach is evaluated with the Computer Controlled Photovoltaic System with a deviation between 2.5 % to 5 % based on tabulated results and graphs.

INTRODUCTION

In seismic data processing and analysis, it takes several hours to understand analogue seismic waveforms from analogue seismographs, even for experienced seismologists to appreciate it hurriedly. Simply due to complexities inherent in the analogue device. While a digital broadband seismograph is continuously recording, the initial motion remains intact and easy to interpret the continuous waveforms [1] and it tends to contain more information. However, a modern digital broadband seismograph at the remote seismic node requires a continuous and reliable energy harvesting system. This digital broadband seismograph expects that the constraints in the photovoltaic (PV) energy harvesting system be optimized to enable continuous power supply. Secondly, reducing the cost of efficient PV energy harvesting systems has been continuously high and challenging. These form the motivation to present a novel approach for continuous and reliable photovoltaic energy harvesting systems at critical remote nodes, enabling the study and monitoring of earth deformation feasible. The proposed analytical model derived from light-dependent resistor (LDR) characteristics to minimize prediction cost while delivering prediction accuracy. Our validation outcomes demonstrate relatively improved match real performance yet relatively simple computational processes. By using the variables of a PV module in Computer Controlled Photovoltaic System and LDR to model the equation for prediction of duty cycle levels to feed the pulse width modulation (PWM) and drive the DC-DC converter. This controlled PV system has an inbuilt maximum power point tracking system (MPPT) to track possible maximum operating points of current and voltage. In addition, critical instances of PV systems can be in partial shading and darkness, where energy storage is the best option for reliable and continuous current through a load. A supercapacitor as energy storage is integrated to enable continuous electrical power at the remote seismic node. An asynchronous buck DC-DC converter is adopted for optimal energy conversion to the supercapacitor and load for both shaded and unshaded periods of the PV module.

The major contributions of this research are:

- We have proposed an optimal maximum possible operating point of voltage and current levels using curve fitting equations.
- We have made possible a less computational MPPT technique with low cost and suitable for a remote seismic node where insufficient funding is always the case.

The remaining part of the article is organized as follows. Section 2 provides the theoretical background on the proposed design of the PV energy harvesting system and its elements. Section 3 describes a typical remote seismic node and subsystems of the proposed PV energy harvesting system. In Section 4, we describe the optimization technique and the implementation. Section 5 presents the experimental results and comparison between the proposed design and the experimental setup, while section 6 finally concludes the paper.

Photovoltaic Energy Harvesting System

A photovoltaic cell is a current source generated from ambient irradiance and temperature change, having diode D connected in parallel. Considering power losses due to internal series R_S and parallel R_P resistances as shown in Figure 1 [2] and available current I_{PV} through the load is shown in Figure 1. Using Kirchoff's Law and applying circuit analysis in Figure 1, the generated current through the load is defined in Eqn. 1, while Figure 2 demonstrates the waveforms across the circuit.

Eqn. 2 and Eqn. 3 express the current I_D through the diode D, I_P being the current through R_P and the generated current at the terminal I_{PV} [3], where I_{PV} could be equally expressed in Eqn. 4.

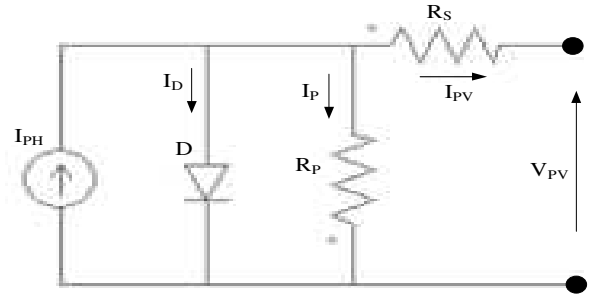

Figure 1. Equivalent Circuit of PV Cell.

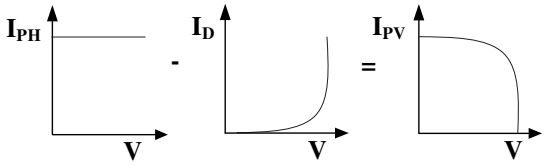

Figure 2. Waveforms of Equivalent Circuit in PV Cell.

$$I_{PV} = I_{PH} - I_D - I_{SH} \quad (1)$$

$$I_D = I_{SAT}\left(exp\left(\frac{q*(V_{PV}+I_{PV}*R_S)}{KT_{Ambient}A}\right) - 1\right) \quad (2)$$

$$I_{PV} = \left(I_{SC,Ref} + k_i * \left(T_{Ambient} - T_{Ref}\right) * \frac{G_{Ambient}}{G_{Ref}}\right) \quad (3)$$

$$V_{PV}(T) = V_{OC,Ref} + k_v * \left(T_{Ambient} - T_{Ref}\right) \quad (4)$$

Where q = electron charge
V_{PV} = Terminal Voltage
K = Boltzmann Constant
$T_{Ambient}$ = Operating Temperature
T_{Ref} = Operating Temperature
A = Ideality Factor
$V_{OC,Ref}$ = V_{OC} at reference temperature and irradiance
$I_{SC,Ref}$ = I_{SC} at reference temperature and irradiance
k_v = Temperature Coefficient of V_{OC}
k_i = Temperature Coefficient of I_{SC}

The expressed equations continuously determine the open-circuit voltage V_{OC}, Short circuit current I_{SC}, and the possible maximum current I_{MAX} and voltage V_{MAX} measurements, as shown in Figure 3. The constraints of solar cells bring down the efficiency and operate away from the maximum operating points of I_{MAX} and V_{MAX}. However, the accurate tracking of this maximum operating point delivers maximum power and directly depends on the DC-DC converter employed in the application.

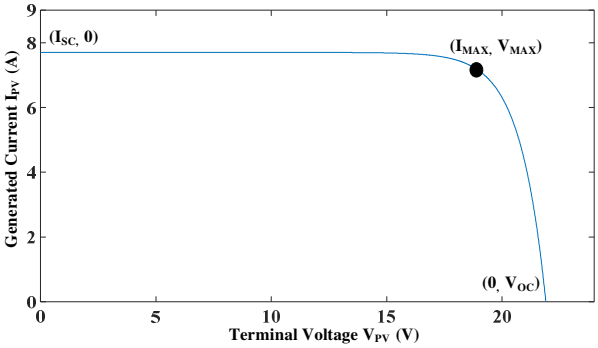

Figure 3. Current and Voltage Relationship with its Maximum Operating Points

Materials and Methods

A typical modern remote seismic node that houses a digital seismograph requires 12 V and 0.8 A DC power supply. The DC power is acquired from ambient harvested solar energy by photovoltaic module with DC-DC converter and energy storage. The energy storage being supercapacitor provides instantaneous energy to the node during shaded periods. In the proposed power solution, the DC-DC converter is optimally controlled using a curve fitting model to energize the remote seismic node and supercapacitor. Figure 4 shows a schematic diagram of MPPT based on a curve-fitting model comprising of a PV module, two voltage sensors to monitor voltage levels across the module, and the supercapacitor. Additionally, a curve-fitting model, which interfaces the LDR and temperature sensor with an algorithm developed in a C programming environment and 8-bit microcontroller to feed the optimal duty cycle across the converter, is implemented.

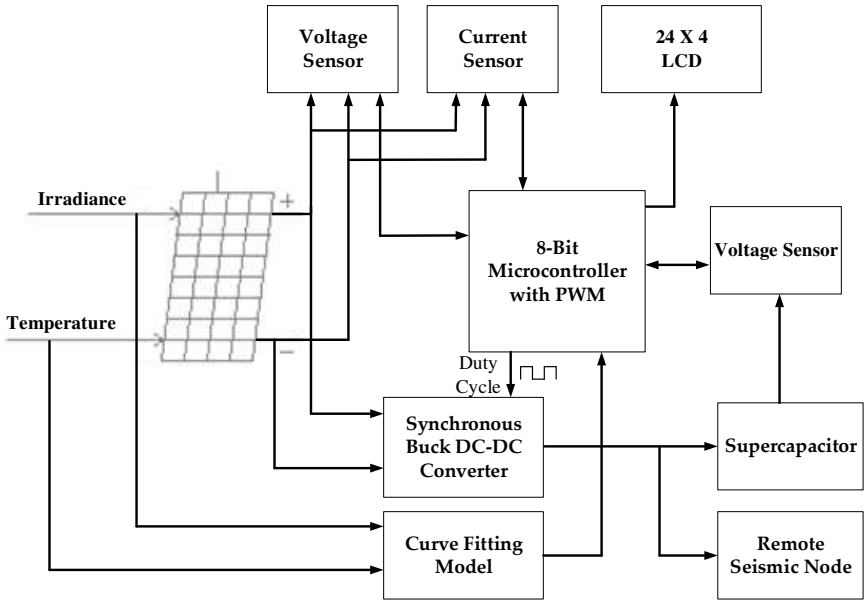

Figure 4. Schematic Diagram of the Proposed Photovoltaic Energy Harvesting System.

Curve Fitting Model for Maximum Power Point Tracking and Implementation

The proposed design adopts a simple sensor of LDR by establishing a correlation between the measurements of LDR and its V_{LDR}, by placing it side by side with a pyranometer for the calibration. The light-dependent resistor exhibits a change in resistance as the ambient irradiance level changes, and the resistance decreases with an increase in the irradiance. Figure 5 shows the LDR connection circuit in the Proteus environment, which controls the irradiance levels that hits it, and the measurements are populated in Table 1.

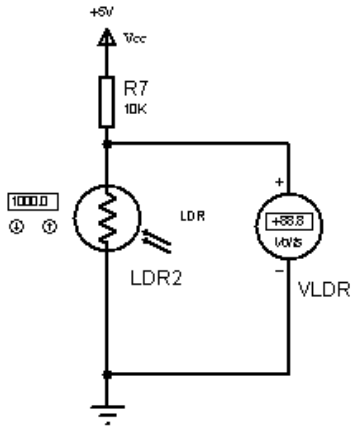

Figure 5. LDR Connection Circuit.

Irradiance (Wm^{-2})	V_{LDR} (V)	Log Irradiance (Wm^{-2})	Log V_{LDR} (V)
10	3.19	1	0.503791
100	0.98	2	-0.00877
200	0.59	2.30103	-0.22915
300	0.44	2.477121	-0.35655
400	0.35	2.60206	-0.45593
500	0.29	2.69897	-0.5376
600	0.25	2.778151	-0.60206
700	0.22	2.845098	-0.65758
800	0.2	2.90309	-0.69897
900	0.18	2.954243	-0.74473
1000	0.16	3	-0.79588

Table 1: Measurements from the LDR Connection Circuit.

The curve in Figure 6 is a bit tricky, where the voltage across the LDR V_{LDR} decreases with the rise in irradiance level, which is expressed in Eqn. 5 and exhibits nonlinearity. The LDR exhibits internal nonlinear characteristics, and the function can be represented in logarithm function for it to demonstrate linearity [148]. The logarithm of the measurements in Table 1 is computed and plotted again, and it took the form of a linear plot in Figure 7 and expressed in Eqn. 6. Where m represents the average slope and c denotes the y axis intercept of the line and constants, while variable y is the output variable based on the change of x.

$$V_{LDR} = \frac{R_{LDR}}{R_{LDR} + 10000} * V_{CC} \quad (5)$$

$$y = m * x + c \quad (6)$$

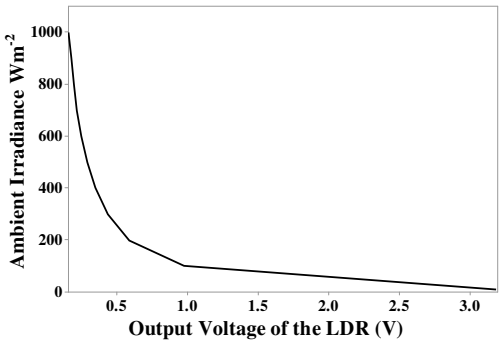

Figure 6. Relationship between Irradiance and V_{LDR}.

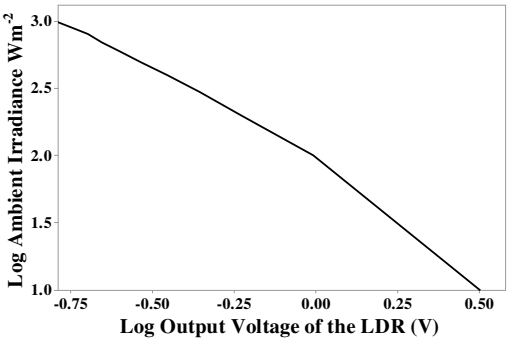

Figure 7. Relationship between Log Irradiance and Log V_L.

The generated current is directly proportional to the ambient irradiance $G_{Ambient}$ as expressed in Eqn. 7. Based on Eqn. 1, and I_D is a function of ambient temperature, and thus varying temperature influences the measurements of I_{MAX}. To obtain maximum power output from PV module, the maximum power point (MPP) needs to be sensed. The relationship between the current and voltage of photovoltaic cell at any operating point can be expressed in Eqn. 8 and Eqn. 9 [6]. Where a unique MPP exists for every combination of ambient irradiance and temperature levels.
The reference irradiance G_{Ref} and Eqn. 7 is replaced with Eqn. 10, when $I_{MPP,Ref}$ is the maximum current of a PV cell at G_{Ref} and T_{Ref} based on the vendor information.

$$I_O \propto G_{Ambient} \tag{7}$$

$$I_{SC} = I_{SC,Ref} * \frac{G_{Ambient}}{G_{Ref}} + k_i * \left(T_{Ambient} - T_{Ref}\right) \tag{8}$$

$$V_{OC} = V_{OC,Ref} + A * V_t * \ln\frac{G_{Ambient}}{G_{Ref}} + \beta\left(T_{Ambient} - T_{Ref}\right) \tag{9}$$

$$I_{MAX} \propto I_{MPP,Ref} * \frac{G_{Ambient}}{G_{Ref}} \tag{10}$$

So, therefore, the operating point of PV cell at I_{MAX} can be expressed in Eqn. 11 and per the fundamental equation Eqn. 8. Similarly, Eqn. 9 is being replaced by Eqn. 12. Where $I_{MPP,\,Ref}$ and $V_{MPP,Ref}$ are the maximum current and voltage, respectively obtained at the G_{REF} and T_{REF} of that particular PV module.

$$I_{MAX} = I_{MPP,Ref} * \frac{G_{Ambient}}{G_{Ref,MPP}} + k_i * \left(T_{Ambient} - T_{Ref,MPP}\right) \tag{11}$$

$$V_{MAX} = V_{MPP,Ref} + A * V_t * \ln\frac{G_{Ambient}}{G_{Ref}} + \beta\left(T_{Ambient} - T_{Ref}\right) \tag{12}$$

To solve Eqn. 11, we have developed a computational code in C programming to compute I_{MAX} and V_{MAX} measurements.

MPPT approaches are the DC-DC converter's key factor, which provides the impedance matching for maximum energy transfer. The proposed synchronous buck DC-DC converter has electrical characteristics tabulated in Table 2.

Parameter	Value
V_{IN}	22.9 V
V_O	12 V
I_O	0.8 A
Switching Frequency F_{SW}	10 KHz
Current Ripple ΔI	30 %
Voltage Ripple ΔV	15 %

Table 2. Buck Converter Parameters.

The selection of an inductor for a buck DC-DC converter is key to its performance due to conduction losses and acts as a low pass filter with the output capacitor. The conduction current flows through the inductor and increases linearly during the on-state of the converter switch.

$$L_{Min} = \frac{V_{OUT} * (V_{IN} - V_{OUT})}{V_{IN} * F_{SW} * \Delta I} = \frac{12 * (22.9 - 12)}{22.9 * 10 * 10^3 * 0.24} = 2.37mH \quad (13)$$

A capacitor is part of the low pass filter, and corner frequency is calculated at low frequency to limit the switching ripples of the buck DC-DC converter. Where the minimum output capacitor C_{OUT} is 1.67uF, the higher the capacitance, the less ΔV across the load.

$$C_{OUT} = \frac{\Delta I}{8 * F_{SW} * \Delta V} = \frac{0.24}{8 * 10 * 10^3 * 1.8} = 1.67uF \quad (14)$$

In the synchronous buck DC-DC converter, two MOSFETs are needed, a low side MOSFET to replace the usual diode and improve the overall efficiency. Comparing Eqn. 15 and Eqn. 16, power losses by the diode are more than the low side MOSFET. Taking into consideration a duty cycle of converter D, the forward drop voltage V_D of a diode and drain-source resistance of a MOSFET R_{DSON}, and usually V_D is extremely greater than the product of R_{DSON} and I_O^2.

$$Losses_{Diode} = V_D * (1 - D) * I_O \quad (15)$$
$$Losses_{Mosfet} = I_O^2 * R_{DSON} \quad (16)$$

Two N-channel MOSFETs of IRF3205 for both high and low sides with RDSON = 8 mΩ and MOSFET driver of IRF2102 were implemented. A controller is synchronized between the two switches to control the output voltage levels and avoid the two switches conducting simultaneously. For optimal performance of the switch, the drain to source VDS of MOSFET should exceed VIN and enable minimum conduction losses.

Pulse width modulation is a technique used to control the duty cycle of a buck DC-DC converter. It offers simplicity, a relatively low noise level, and a faster response controller than other controllers employed in converter applications [7]. These characteristics are good options for a remote seismic node due to the low noise exhibited in the energy harvesting system.

A supercapacitor is like a conventional capacitor but with superior energy storage and capacitance with relatively smaller, lower internal resistance and more extended lifecycle [8]. The terminal voltage V_{Scap} and charging current $I_{Scap}(t)$ into the supercapacitor at time t can be expressed in Eqn. 17 and Eqn. 18, respectively [8].

$$V_{Scap}(t) = V_{IN} + \left[\left(V_{Scap}(0) - V_{IN} \right) * exp\left(-\frac{t}{R * C} \right) \right] \quad (17)$$

$$I_{Scap}(t) = \left(\frac{V_{IN}}{R}\right) * exp\left(-\frac{t}{RC}\right) \quad (18)$$

In this proposed work, KAMCAP brand of supercapacitor with 1000 F and 2.7 V characteristics were selected, and five supercapacitors were combined for the power solution at remote seismic node.

$$\frac{1}{C_{Total}} = \frac{1}{C_1} + \frac{1}{C_2} + \frac{1}{C_3} + \frac{1}{C_4} + \frac{1}{C_5} = \frac{5}{1000}, \qquad C_{Total} = 200\ F$$

Total Capacity E_{Total} in Watts per hour at initial voltage V_{Min} and final voltage V_{Max} can be expressed as

$$E_{Total} = \frac{1}{2} * C_{Total} * \ (V_{Max} - V_{Min})^2 = \frac{1}{2} * 200 * (13.5 - 0)^2 = 36{,}450\ J = 607.5\ Wh$$

Figure 8 shows the synchronous buck DC-DC converter circuit that converts input voltage to the desired voltage for the load in Proteus. While Figure 9 is the novel optimal energy harvesting system consisting of 8-bit Arduino Uno microcontroller, the LDR, temperature sensor, and the synchronous buck DC-DC converter.

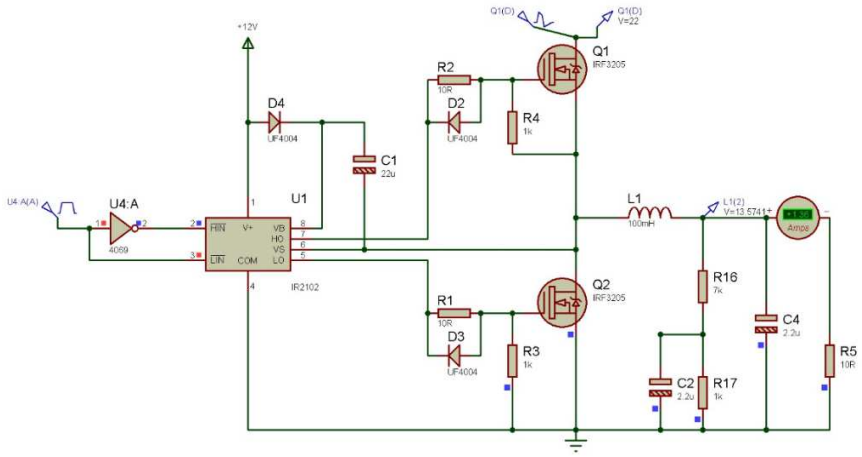

Figure 8. Synchronous Buck DC-DC Converter Design in Proteus Program

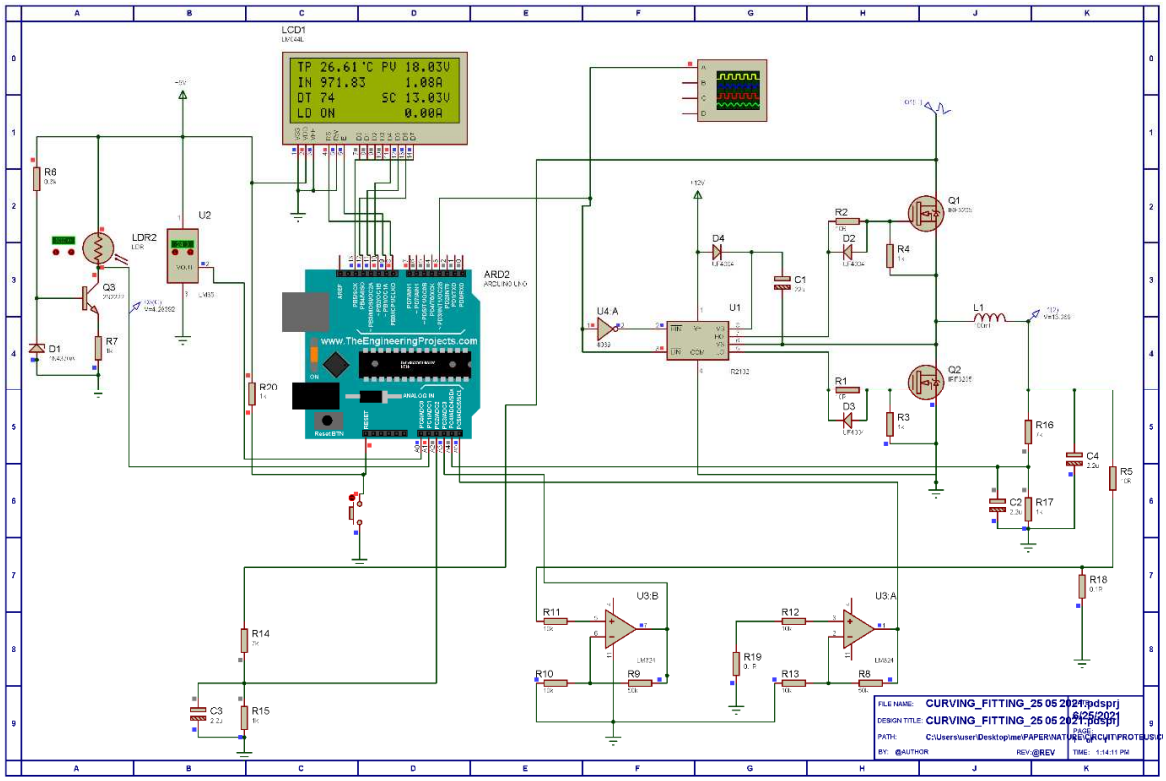

Figure 9. The Proposed Photovoltaic Energy Harvesting System at Remote Seismic Node

Results and Analysis

Figure 10 demonstrates the varying duty cycle levels controlled by the curve fitting model integrated with the algorithm developed with C programming and loaded on the microcontroller.

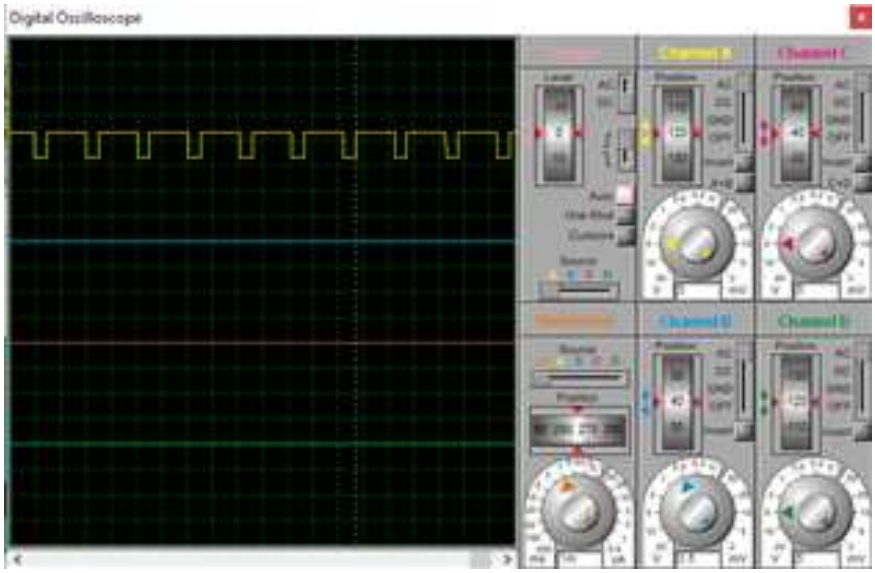

Figure 10. Waveform of Duty Cycle by the 8-bit Microcontroller

The experimental setup (Figure 11) is made up of Computer Controlled Photovoltaic System to evaluate the optimal PV harvesting system for the remote seismic node. The Figure 11 contains a pyranometer for measuring ambient irradiance, temperature sensor for temperature observations, DC-DC converter-based MPPT, and 120 W PV module. As well as computer system, which has an in-built interface to vary all the input parameters of the module, observe all the output parameters and acquisition of data. The experiment was conducted indoor where the PV lamps supply irradiance with intensity and frequency spectrum like the sunlight. Current and voltage behaviour obtained from the PV Controlled Computer System is reported in Figure 12 for different ambient irradiance.

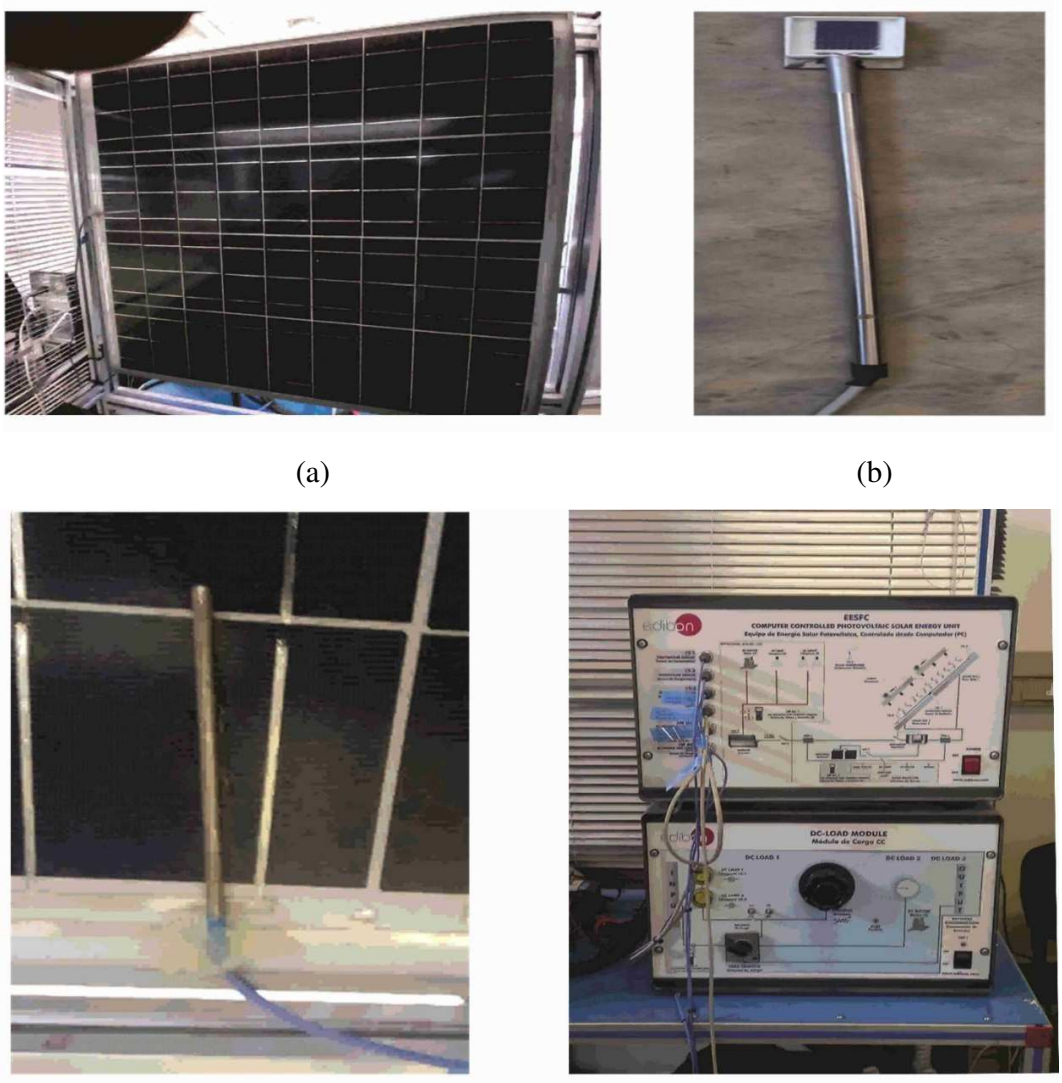

(a) (b)

(c) (d)

Figure 11. Experimental Setup (a) 120 W PV Module, (b) Pyranometer (c) Temperature Sensor (d) DC-DC Converter with MPPT system.

500 Wm^{-2} and 25^0C		300 Wm^{-2} and 25^0C		100 Wm^{-2} and 25^0C	
V_O	I_O	V_O	I_O	V_O	I_O
0	3.8708	0	2.32248	0	0.77416
3	3.704995	3	2.221795	3	0.6
6	3.65	6	2.17	6	0.6
9	3.64	9	2.17	9	0.55
12	3.55	12	2.1	12	0.52
15	3.55	15	2.1	15	0.51
18	3.3906	18	1.946964	18	0.398644
19.8	0	19.0	0	18.4	0

Table 3. Measurements acquired from PV Controlled Computer System

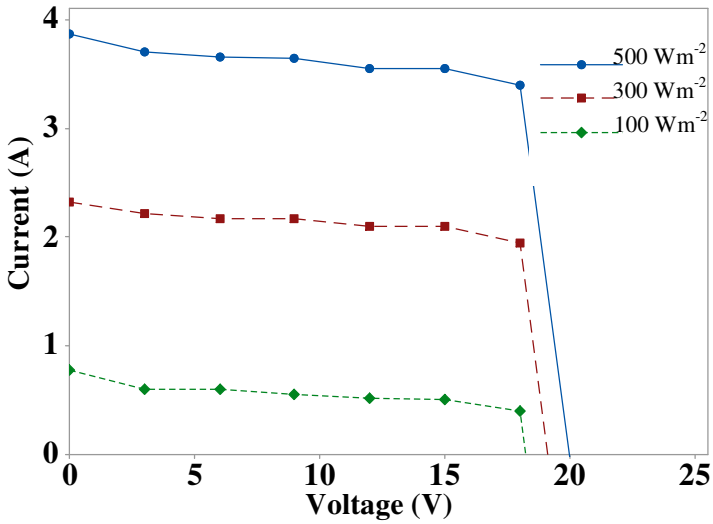

Figure 12. Current and Voltage behaviour obtained from the PV Controlled Computer System.

		Experimental Measurement			Proposed Measurement		
$T_{Ambient}$ (^0C)	$G_{Ambient}$ (Wm^{-2})	I_{MAX} (A)	V_{MAX} (V)	Duty Cycle	I_{MAX} (A)	V_{MAX} (V)	Duty Cycle
25	1000	5.9494	18.994	0.71075	5.67	18.528	0.73628
25	800	4.55952	18.994	0.71075	4.26552	18.45	0.7395
25	600	3.16964	18.994	0.71075	2.77564	18.1	0.75
25	500	2.4747	18.994	0.71075	2.19	18.1	0.75
25	400	1.77976	18.994	0.71075	1.58576	17.9	0.75429
25	300	1.08482	18.994	0.71075	0.9	17.8	0.77193
25	200	0.38988	18.994	0.71075	0.35	17.8	0.77193
25	100	0.30506	18.994	0.71075	0.1	17.8	0.78107
26	1000	5.9517	18.867	0.71554	5.59	17.6	0.73743
27	1000	5.954	18.74	0.72038	5.59	17.8	0.74157

Table 4. Comparison of the Performances of PV Controlled Computer System and Proposed Model.

The MPPT efficiency η_{MPPT} of both the experimental setup and the proposed PV energy harvesting system can be evaluated by using Eqn. 19 [10], where the VMPP and IMPP of the considered PV module are 17.2 V and 7 A, respectively. The measurements acquired from PV Controlled Computer System is reported in Table 3. The performances of both systems were compared using Table 4 and Figure 13.

$$\eta_{MPPT} = \frac{P_{MPPT}}{P_{PV}} = \frac{V_{MAX} * I_{MAX}}{V_{MPP} * I_{MPP}} * 100\ \% \quad (19)$$

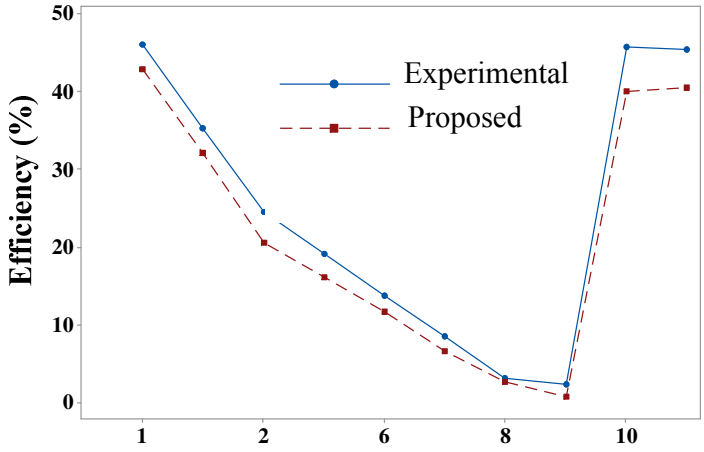

Figure 13. Efficiency Comparison between the PV Computer Controlled and Proposed MPPT based Curve Fitting Model.

Conclusions

The curve fitting model with LDR and temperature sensor LM35 have been proposed to predict duty cycle across synchronous buck converter to track optimal power and supercapacitor to serve as energy storage. The use of a Supercapacitor was proposed due to its relatively higher power density and longer lifecycle. Comparing the experimental results with our curve-fitting model approach, the outcomes revealed justified and inexpensive power solutions to deploy at a remote seismic node for continuous and long-term seismic data acquisition. The evaluation of our approach deviated about 2.5 % to 5 % from the experimental setup, which is expensive, complex and bulky for remote seismic node. The developed model can support PV energy harvesting system with different combinations of ambient irradiance and temperature levels based on results obtained from tabulated data and graphs.

References

[1] J. M. H. Menu, "A digitization noise model for earthquake strong motion," in *Proceedings, Workshop on Investigation of Strong Motion Processing Procedures*, Rome, 1985.

[2] T. Pei and X. Hao, "A Fault Detection Method for Photovoltaic Systems," *Energies,* vol. 12, no. 1712, p. 16, 2019.

[3] M. Aidoud, C. Feraga, M. Bechouat, M. Sedraoui and S. Kahla, "Development of Photovoltaic Cell Models Using Fundamental Modeling Approaches," *Energy Procedia,* vol. 162, no. 2019, pp. 263-274, 2019.

[4] R. Caponetto, G. Dongola and L. Fortuna, Fractional Order Systems Modeling and Control Applications, Singapore: World Scientific Scientific Publish Co, Pte, Ltd, 2010.

[5] T. U. Townend, "A Method for Estimating the LongTerm Performance of Direct-Couple Photovoltaic Systems," University of Wiscousin, Wiscousin, 2010.

[6] F. Z. Kessaissiaa, A. Zegaoui, A. H. Arab, L. Loukarfi and M. Aillerie, "Comparison of Two PV modules Technologies Using Analytical and Experimental Methods," in *International Conference on Technologies and Materials for Renewable Energy, Environment and Sustainability*, 2015.

[7] M. W. Kim and J. J. Kim, "A PWM/PFM Dual-Mode DC-DC Buck Converter with Load-Dependent Efficiency-Controllable Scheme for Multi-Purpose IoT Applications," *Energies,* vol. 14, no. 960, p. 14, 2021.

[8] B. Y. Kim, S. Sy, A. Yu and J. Zhang, "Electrochemical Supercapacitors for Energy Storage and Conversion," in *Energy Storage Electrochemical Storage*, John Wiley & Sons, Ltd, 2015, p. 25.

[9] R. Asnawi, D. Nurhadiyanto, Z. Arifin and A. Asmara, "The Characteristic of Supercapacitors Circuit as a Future," *Journal of Physics,* vol. 1140, no. 2018, p. 10, 2018.

[10] H. Sharma, A. Haque and Z. A. Jaffery, "An Efficient Solar Energy Harvesting System for Wireless Sensor Nodes," in *2nd IEEE International Conference on Power Electronics, Intelligent Control and Energy Systems*, Delhi, 2008.

[11] C. Djekic, M. Brkovic and A. Roy, "High Frequency Synchronous Buck Converter for Low Voltage Applications," in *29th Annual IEEE Power Electronics Specialists Conference (Cat. No.98CH36196)*, Fukuoka, 1998.

[12] D. M. Sable, F. C. Lee and B. H. Cho, "A Zero-Voltage-Switching Bidirectional Battery Charger/Discharger for the NASA EOS Satellite," in *APEC '92 Seventh Annual Applied Power Electronics Conference and Exposition*, Boston, 1992.

[13] T. Markvart, Solar Electricity, Wiley, 2000.

[14] M. A. Habib, S. Said, M. D. El-Hadidy and I. Al-Zaharna, "Optimization Procedure of a Hybrid Photovoltaic Wind Energy System," *Energies,* vol. 24, no. 11, pp. 919-929, 1999.

[15] W. N. V. Wieringen, "Lecture Notes on Ridge Regression," Creative Commons, 2020.

[16] S. Nikam, L. Ragha and S. Kulkarni, "Neuro Fuzzy Approach for Financial Forecasting," *International Journal of Research in Advent Technology,* vol. 1, no. 2, pp. 49-65, 2013.

Acknowledgments

Authors are indebted to Botswana International University of Science and Technology. The authors are thankful to BIUST management for the support.

Author contributions

All co-authors of this manuscript have equally contributed to the content of this manuscript. **Dauda Duncan** – Conceived idea, designed and performed the simulation work, and took the lead in writing the manuscript**. Adamu Murtala Zungeru** – Senior author who conceived the idea, supervised the project, and co-written the manuscript. **Mmoloki Mangwala** – provided critical feedback and helped shape the research, analysis, and manuscript. **Bakary Diarra** – provided critical feedback and helped shape the research, analysis, and manuscript.

Competing interests
The authors declare no competing interests.

Data availability
There is no external data used for this research

Additional information
Correspondence and requests for materials should be addressed to Adamu Murtala Zungeru.